

LATE PLIOCENE VARIATION IN NORTHERN  
HEMISPHERE ICE SHEETS AND NORTH ATLANTIC  
DEEP WATER CIRCULATION

M. E. Raymo,<sup>1,2</sup> W. F. Ruddiman,<sup>1</sup> J. Backman,<sup>3</sup>  
B. M. Clement,<sup>4,5</sup> and D. G. Martinson<sup>1</sup>

*Abstract.* High-resolution records of  $\delta^{18}\text{O}$ ,  $\delta^{13}\text{C}$ , and percent  $\text{CaCO}_3$  from the late Pliocene North Atlantic (Deep Sea Drilling Project sites 607 and 609) are presented and oxygen isotope stages are formalized back to stage 116 at 2.73 Ma. From 2.8 to 1.6 Ma, the interval studied, variations in these records were dominated by the 41-kyr component of orbital obliquity. Significant variation at the orbital frequencies of eccentricity (96-kyr) and precession (23-kyr) are observed in the  $\delta^{18}\text{O}$  record between 1.6 and 2.1 Ma, but not before. Prior to 2.4 Ma (stage 100),  $\delta^{18}\text{O}$  variations suggest ice sheet growth 1/4 to 1/2 as large as late Pleistocene ice volumes; however, these events are below the threshold needed to result in extensive ice-raftering to the open North Atlantic Ocean. After 2.4 Ma, ice sheets appear to be, on average, 1/2 as large as those of the late Pleistocene. The  $\delta^{13}\text{C}$  record indicates that some glacial suppression of North Atlantic Deep Water occurred both before and after 2.4 Ma and that glacial-interglacial transfers of  $^{12}\text{C}$  between the continents and oceans appear to have been larger in the late Pliocene relative to the

late Pleistocene. In addition, the strong 23-kyr power observed in  $\delta^{13}\text{C}$  between 2.75 and 2.10 Ma suggests that deep-sea circulation (or changes in biomass) is controlled, in part, by climatic variations unrelated to ice sheets.

INTRODUCTION

In the late Pliocene a fundamental change in the Earth's climate occurred when continental size ice sheets began to grow and shrink over vast areas of North America and Eurasia. This cooling, which began ~3.1 m.y. ago [Backman and Pestiaux, 1986; Raymo et al., 1986; Einarsson and Albertsson, 1988], led to the accumulation of gradually larger ice sheets, culminating in the first extensive episode of ice-raftering in the open North Atlantic at 2.4 Ma [Backman, 1979; Shackleton et al., 1984].

We examine, over a range of latitudes and depths, the late Pliocene isotope and carbonate records of this major climatic transition. We present two major results. First, the early Matuyama, from 2.4 to 1.6 Ma, was characterized by ice volume changes primarily at the 41-kyr rhythm of orbital obliquity. However, minor variations at the orbital periods of eccentricity and precession occurred between 2.1 Ma and 1.6 Ma. Second, the interval prior to large-scale glaciation at 2.4 Ma is also characterized by variations at the 41-kyr rhythm which gradually increased in amplitude toward 2.4 Ma. These data confirm the dominance of the 41-kyr obliquity cycle in the record of global ice volume back to 2.8 Ma. Further, we use this observation as the basis for extending the oxygen isotope time scale of Ruddiman et al. [1986a] back to this time.

Three North Atlantic Deep Sea Drilling Project (DSDP) sites (Figure 1) forming a latitudinal transect as well as a depth transect were used in this study. Site 607 (3427 m below sea level (mbsl)), the southernmost of the three sites, is located on the western flank of the Mid-Atlantic Ridge (MAR) in the core of North Atlantic Deep Water (NADW). This site sits under the northern limb of the North Atlantic Current at the northern edge of the subtropical gyre. Site 609 (3884 mbsl) is located on the eastern flank of the MAR and is today influenced by

<sup>1</sup> Lamont-Doherty Geological Observatory and Department of Geology, Columbia University, Palisades, New York.

<sup>2</sup> Now at Department of Geology, Monash University, Clayton, Victoria, Australia.

<sup>3</sup> Department of Geology, University of Stockholm, Stockholm, Sweden.

<sup>4</sup> Ocean Drilling Program, Texas A and M University, College Station.

<sup>5</sup> Now at Department of Geology, Florida International University, Miami.

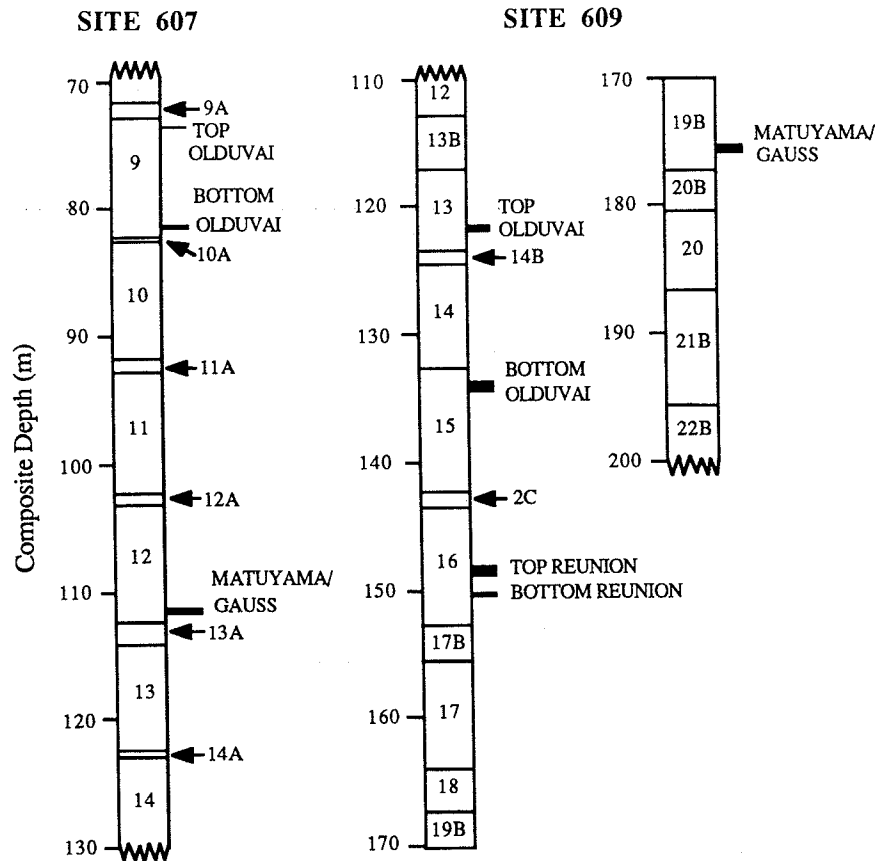


Fig. 2. Composite depth sections for sites 607 and 609 generated by splicing sections from the offset hole across core breaks in main hole. The composite depth ranges of magnetic reversal datums, as determined from carbonate and visual correlations between the main and offset holes, are indicated by black bars to the right of the composite sections.

and 609B, the Pliocene interval contained a number of underrecovered or disturbed cores in both holes. In the composite depth model, summarized in Table 2, we were able to splice only four of the nine core breaks in this interval. The 15/16 core break was spliced using a section from hole

609C. At the end of core 609-18, our record switches to core 609B-19, maintaining the cored DSDP offset. From this point on, 609B is the main hole, with a section from hole 609 used to splice over the 20B/21B core break.

Of these four splices, the top of the 15/16 splice is

TABLE 1. Composite Depth Model for Late Pliocene Section of Site 607

Interval in Hole 607 <sup>a</sup>	Interval in Hole 607A <sup>a</sup>	Composite Depth, m
9-7-31	10-4-30	82.01
10-1-7	10-4-90	82.61
10-7-27	11-4-1	91.81
11-1-5	11-4-105 <sup>b</sup>	92.85
11-7-8	12-3-105	101.88
12-1-5	12-4-91	103.24
12-7-7	13-4-31	112.26
13-1-78	13-5-61	114.06
13-7-21	14-4-135	122.49
14-1-5	14-5-45.5 <sup>b</sup>	123.09

<sup>a</sup> Depth intervals are given in Deep Sea Drilling Project format: core-section-depth in section (cm).

<sup>b</sup> Uncertainty in exact splice depth.

TABLE 3. (continued)

Datum	Hole	Depth Range of Reversal <sup>a</sup>	Equivalent Depth Range <sup>a,b</sup>	Data Source <sup>c</sup>
Top of Reunion (continued)	609	16-4-20/16-4-98	---	1
	609B	not recovered	---	
	Composite 609	16-4-20/16-4-98		
Bottom of Reunion	607		---	
	607A	not recovered	---	
	Composite 607			
	609	16-5-20/16-5-98	---	1
	609B	17-1-98/17-1-146	609-16-5-68/16-5-116	1
	Composite 609	16-5-68/16-5-98		
Matuyama/ Gauss	607	12-5-145/12-6-105	---	3
	607A	13-3-97/13-4-55	607-12-6-73/12-7-31	3
	Composite 607	12-6-73/12-6-105		
	609	19-2-68/19-2-135	?	1
	609B	19-6-50/19-6-98	---	3
	Composite 609B	19-6-50/19-6-98		
Top of Kaena	607	14-5-25/14-5-66	---	3
	607A	15-2-100/15-3-97	607-14-4-130/14-5-127	1
	Composite 607	14-5-25/14-5-66		
	609	not recovered	---	
	609B	23-6-140/24-1-98	---	3
	Composite 609B	23-6-140/24-1-98		
Bottom of Kaena	607	14-6-145/15-1-34	---	3
	607A	15-4-97/15-5-97	607-14-6-127/15-1-22	1
	Composite 607	14-6-145/15-1-22		
	609	24-1-98/24-2-138	?	1
	609B	24-4-98/24-5-106	---	1
	Composite 609B	24-4-98/24-5-106		
Top of Mammoth	607	15-3-25/15-3-84	---	3
	607A	not recovered	---	
	Composite 607	15-3-25/15-3-84		
	609	not recovered	---	
	609B	25-5-102/25-6-42	---	3
	Composite 609B	25-50102/25-6-42		
Bottom of Mammoth	607	15-5-133/15-6-23	---	3
	607A	not recovered	---	
	Composite 607	15-5-133/15-6-23		
	609	not recovered	---	
	609B	26-5-11/26-5-111	---	3
	Composite 609B	26-5-11/26-5-111		
Gauss/ Gilbert	607	16-3-97/16-4-97	---	1
	607A	18-1-97/18-2-97	607-16-3-7/16-4-7	1
	Composite 607	16-3-97/16-4-7		
	609	26-2-100/26-3-100	609B-27-5-66/27-6-66	1
	609B	27-6-18/27-6-108	---	3
	Composite 609B	27-6-18/27-6-66		

<sup>a</sup> Depth ranges are given in Deep Sea Drilling Project format: core-section-depth in section (cm).

<sup>b</sup> Correlative depths of magnetic reversals measured directly in the offset hole and then transferred by CaCO<sub>3</sub> or visual correlations into the primary hole used to form the composite depth sequence.

<sup>c</sup> 1, Clement and Robinson [1986]; 2, Clement and Kent [1986]; 3, this paper.

TABLE 4. Depth Ranges of Biostratigraphic Datums

Datum	Hole 607	Hole 609 (609B)	Hole 552A
<i>D. brouweri</i> (LAD)	9-6-75/9-6-149	15-2-44/15-4-44	8-1-29/8-1-39
<i>D. triradiatus</i> acme (FAD)	10-6-52/10-6-77	16-5-95/16-6-145	---
<i>D. pentaradiatus</i> (LAD)	12-3-75/12-3-149	(19-5-90/19-5-120)	9-2-121/9-3-21
<i>D. surculus</i> (LAD)	12-2-48/12-4-48	(19-6-130/19-7-10)	9-3-41/9-4-11
<i>D. tamalis</i> (LAD)	13-3-117/13-4-0	(21-2-1/21-2-31)	10-1-21/10-1-91
<i>N. pachyderma</i> (s) acme FAD	9-1-136/9-2-1	13-6-61/13-6-91	7-3-37/7-3-53
<i>G. inflata</i> (FAD)	10-4-31/10-4-53	16-3-31/16-3-61	8-3-40/8-3-52
<i>N. atlantica</i> (LAD)	12-1-16/12-1-31	(19-1-61/19-1-91)	9-1-147/9-2-5
<i>G. puncticulata</i> (LAD)	12-1-31/12-1-53	(19-3-91/19-3-121)	9-2-45/9-2-77

Depth ranges are given in Deep Sea Drilling Project format: core-section-depth in section (cm).

some cases, reversals are determined only to the 1.5-m shipboard sample spacing, but in others the uncertainty in the depth placement of reversals has been narrowed significantly. Half of all reversals identified in the late Pliocene sections of sites 607 and 609 were found at more than one hole at each site; hence, we were able to further narrow depth ranges of these reversals using the between-hole correlations discussed in the previous section. This was done by correlating the depth range of the reversal in the offset hole into the main, or composite, hole and using the overlap in the ranges to further narrow the uncertainty in the placement of the reversal. In cases where the reversal in the offset hole was very near an interval that was used in the composite depth section (i.e., to splice across a core break in the main hole), the between-hole correlations were excellent and errors in transferred depth ranges were probably less than 5 cm. Reversals further away from sections used in the composite section may have slightly greater uncertainties as to their correlative depths in the main hole. At site 609, the Matuyama/Gauss and lower Kaena reversals were identified in both holes, but because we were not able to make carbonate or visual correlations between the two holes, correlative depths for these reversals could not be determined.

Equivalent depth ranges for reversals found in both holes are listed in Table 3. In all but two of these cases, the overlap in the depth ranges could be used to define a narrowed "composite depth range" of the reversal (also listed in Table 3). The two exceptions are the top of the Olduvai at site 609 and the top of the Kaena at site 607. In these two instances, the projected range from the offset hole is larger than the uncertainty range in the main hole; hence, the composite depth range equals the depth range measured in the main hole. Depth levels for hole 552A magnetic reversals can be found in the work of Krumsiek and Roberts [1984]. In all cases, we use the midpoint of the determined range of a reversal to construct magnetic time scales.

An important difference between earlier magnetic results for site 607 [Clement and Robinson, 1986] and the results presented here is in the identification of the lower boundary of the Olduvai. During construction of the composite section, we found that our visual and carbonate correlations between holes 607 and 607A were inconsistent with the magnetic correlation of the bottom of the Olduvai in these holes. Additional magnetic work in hole 607A confirmed that the actual Olduvai reversal lay ~1.5 m higher in the section than had been previously reported, between 8275 and 8310 cm (DSDP subbottom depths) rather than between 8396 and 8420

cm (Figure 3). The positively magnetized samples between 8396 and 8420 cm cannot be correlated with either the Reunion or Gilsa subchrons. Biostratigraphic and carbonate correlations to site 609 indicate that the Reunion event would fall significantly deeper at site 607. Similarly, a very short polarity subchron identified just above the Olduvai subchron at site 609 [Clement and Kent, 1986/1987] is believed to represent the Gilsa subchron. The interpolated age of this event (1.55 Ma; Figure 3) is very close to the radiometric age of a normally polarized lava from east Iceland ( $1.58 \pm 0.2$  Ma [Watkins et al. 1975; Mankinen and Dalrymple, 1979]) originally proposed to represent the Gilsa [McDougall and Wensink, 1966]. By contrast, our event falls slightly below the Olduvai subchron and thus may be indicative of either complex transitional field behavior or a very brief, previously unrecognized reversal. We have also observed this magnetic excursion at holes 609, 609B, and 611 (Figure 3).

Nine nannofossil and foraminiferal datums are recognized and their depth ranges at each site are listed in Table 4. The published ages of these datums are listed in Table 5. A detailed discussion of the foraminiferal datums can be found in the work of Weaver and Clement [1986] and of the nannofossil datums in the work of Backman and Pestiaux [1986]. In this paper, we will use the time scale developed in the next section to further refine the ages of magnetic and biostratigraphic datums at each site.

#### TIME SCALE DEVELOPMENT

Site 607 provides the first continuous, high-sedimentation rate record from the late Pliocene (~2.8 Ma) to present. In this section, we extend the oxygen isotope time scales developed for the late Pleistocene [Imbrie et al., 1984] and early Pleistocene [Ruddiman et al., 1986a; this issue] back to 2.75 Ma using the orbital tuning methods described by Imbrie et al. [1984]. To do this, we rely almost entirely on the oxygen isotopic record from site 607, where we have recovered a complete sediment record for this time interval with splices across all core breaks. The proposed time scale is named TP607.

The  $\delta^{18}\text{O}$  record of site 607 is plotted to depth and to age in Figures 4a and 4b. Ages were derived by linear interpolation between the bottom of the Jaramillo (0.98 Ma), top of the Olduvai (1.66 Ma), Matuyama/Gauss boundary (2.47 Ma), and top of the Kaena (2.92 Ma); (ages are from Berggren et al. [1985]). The isotopic data show obvious

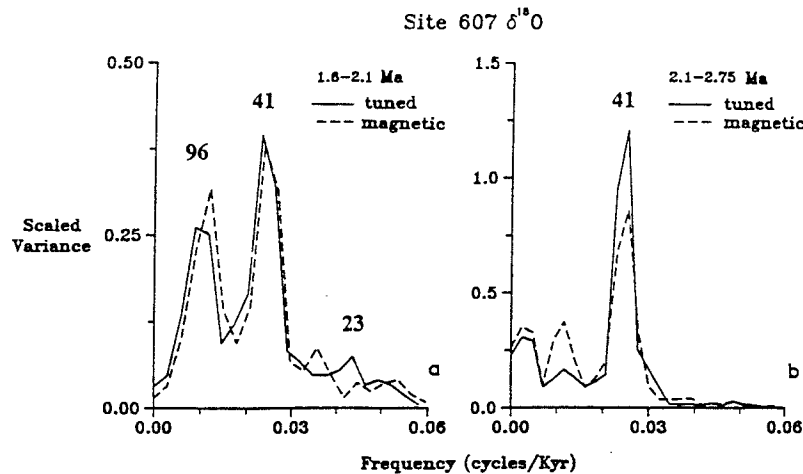


Fig. 5. Tuned and untuned spectra of site 607  $\delta^{18}\text{O}$  from (a) 1.6-2.1 Ma and (b) 2.10-2.75 Ma. Untuned spectra are generated using magnetic datums listed in text. While spectra from both intervals are dominated by the 41-kyr period of obliquity, the spectra from 1.6 to 2.1 Ma show a greater fraction of the total variance concentrated at higher and lower frequencies. All spectra in this paper are generated from evenly interpolated data with the Blackman-Tukey method of spectral analysis using 1/3 lags and no prewhitening. Since the height of confidence interval increases as the frequency decreases, we have labeled peaks that are significant at 90% confidence interval. Band width (bw) equals 0.007.

frequencies (Figure 5a). The filter of the 41-kyr component is correspondingly weaker over this interval. Nevertheless, the spectra in Figure 5 establish the dominance of the 41-kyr cycle of climate modulation back to 2.8 Ma.

We use the concentration of power at orbital frequencies to refine the magnetic time scale by using the tuning methods described by Imbrie et al. [1984] and Martinson et al. [1987]. This method makes two assumptions. First, we assume that individual  $\delta^{18}\text{O}$  cycles in our data can be associated with specific orbital cycles using a fixed time lag. For "tilt" tuning, we use an 8-kyr lag of  $\delta^{18}\text{O}$  behind obliquity forcing as has been demonstrated for the late Pleistocene [Imbrie et al., 1984]. Similarly, for "precession" tuning, we use a 5-kyr lag [Imbrie et al., 1984]. Second, we assume that we are not missing any cycles (i.e., there are no hiatuses in the sediment record of site 607). Of these two assumptions, the second one is the most vulnerable and could result in the largest errors. The tuning of the late Pleistocene records [e.g., Imbrie et al., 1984] involved a number of records from different areas; therefore, anomalies or hiatuses in any one record were easily identified by comparison with the others. Few high-quality records from the late Pliocene are available to compare to site 607, especially over the interval from 2.1 to 1.6 Ma. Thus, while we avoid hiatuses at core breaks by splicing, there may still be unidentified hiatuses in the sediment record unrelated to the coring process. We will compare our records to others from this interval later in this section.

#### Tuning (2.10-2.75 Ma)

We began the tuning process between 2.10 and 2.75 Ma. Each  $\delta^{18}\text{O}$  maxima/minima is easily correlated to the tilt minima/maxima nearest in age [Berger, 1978]. In Figure 6, the data are plotted to the tuned time scale. This correlation between the  $\delta^{18}\text{O}$  record and the obliquity forcing predicts an

age of 2.48 Ma for the Matuyama/Gauss reversal, in exact agreement with the age given by  $^{40}\text{K}$ - $^{40}\text{Ar}$  measurements [Mankinen and Dalrymple, 1979].

However, this agreement is not definitive proof of our correlation between the orbital record and the  $\delta^{18}\text{O}$  record. With the 2% error cited on radiometric dates (50 kyr at 2.48 Ma), the  $\delta^{18}\text{O}$  record could be translated by one full climate cycle in either direction, and the tuned age of the reversal would still be within the radiometric margin of error. However, an additional test of our correlation is provided by the orbital record itself.

Obliquity cycles between 2.1 and 2.8 Ma are not always 41-kyr long but vary in duration from 36 to 48 kyr. Thus, the amount of sediment deposited within any one climate cycle should also vary. For an average sedimentation rate of 4.5 cm/kyr, the difference in the amount of sediment deposited between a 36-kyr cycle and 48-kyr cycle would be about 54 cm. We ran a series of tests, using the 0.5-m.y. interval between 2.1 and 2.6 Ma, in which the correlations between the sediment record and the orbital forcing were translated up and down by one and two cycles. Each of these five potential correlations (including the initial correlation) was evaluated in four ways (Table 6). First, we calculated sedimentation rates between each  $\delta^{18}\text{O}$  maxima and minima and determined the variance and standard deviation of the sedimentation rates for each correlation. Overall, distortions in sedimentation rates were minimized when the glaciation associated with the Matuyama/Gauss boundary was correlated to the tilt minima at 2489 kyr. Half-cycle sedimentation rates exhibited the least variance and smallest standard deviations with this correlation (Table 6).

We also used the objective, nonlinear method of Martinson et al. [1982] to optimize the correlation between the orbital record of tilt and the  $\delta^{18}\text{O}$  record. The resulting correlation coefficient value reflects the degree of similarity

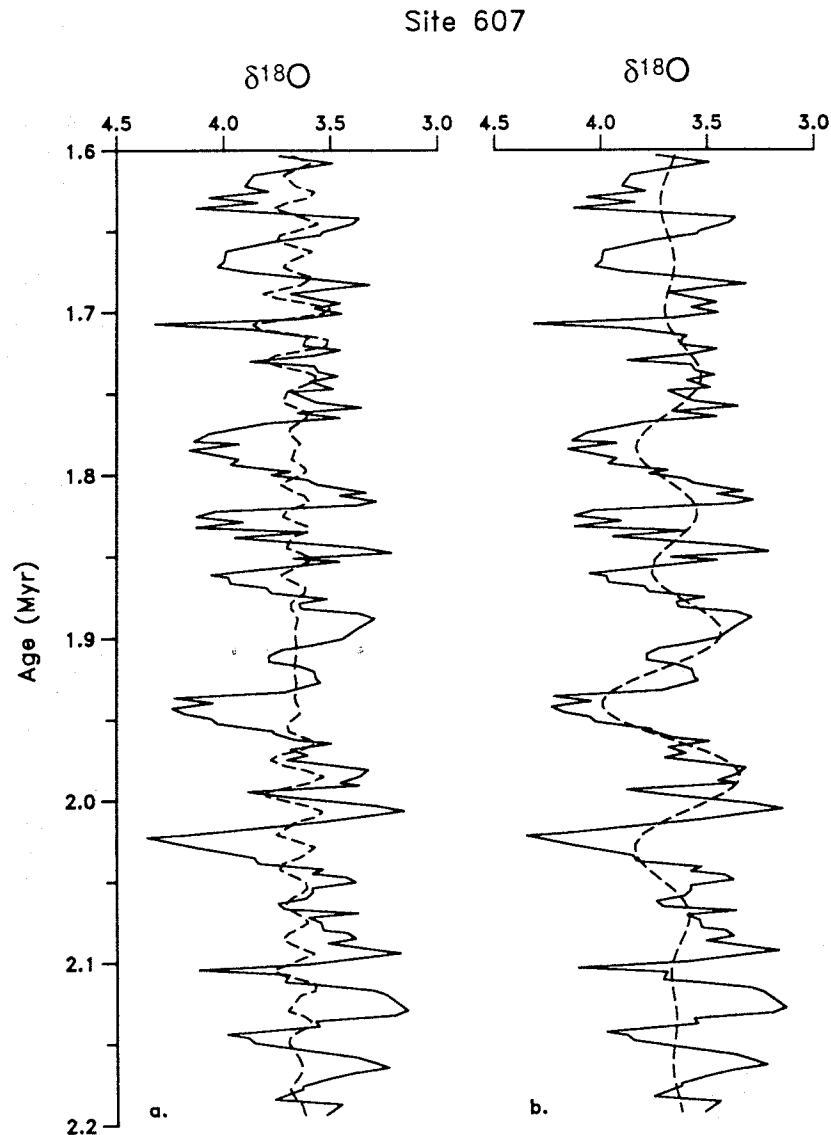


Fig. 8. Values of  $\delta^{18}\text{O}$  plotted to magnetic time scale with filters of (a) 21-kyr and (b) 96-kyr components of the record superimposed (dashed line). Filters are generated from spectra of the 1.6- to 2.2-Ma interval using magnetic time scale. Units for data and filters are the same.

power can be observed in the paleomagnetic spectra in Figure 5a, although it is not strongly concentrated into any one frequency band. In Figure 8a, we have superimposed the untuned 21-kyr (precession) filter from Figure 5a on the  $\delta^{18}\text{O}$  data (filter extends from 17 to 25 kyr). Between 1.65 and 1.80 Ma, and also between 1.95 and 2.15 Ma, precessional effects do appear to be present in the data. Thus, although the dominant period is still 41 kyr within this interval (Figure 5), we have adjusted our tuning strategy to include the effects of precessional forcing. By tuning to precession, more of the high-frequency variance is concentrated directly under the precessional band. We used as a tuning target a composite orbital record generated by adding the precessional forcing (inverted and at half strength) to the obliquity forcing, with the

appropriate lags. This target curve (shown in Figure 9) thus reflects the continued dominance of 41 kyr in the  $\delta^{18}\text{O}$  signal while accounting for some precessional influence.

Before tuning, we fixed the ages at both ends of the 1.6- to 2.1-Ma interval. The upper boundary of the Pliocene, and thus the youngest portion of the Olduvai, was dated by Ruddiman et al. [1986a; this issue] in their time scale for the early Pleistocene. In the time scale developed here, a continuation of the Ruddiman et al. [1986a; this issue] work, we thus correlate (with an 8-kyr lag) the glacial just preceding the upper Olduvai reversal to the tilt minimum at 1668 kyr. This gives a tuned age of 1.65 Ma for this reversal. The 2.1-Ma level was constrained by tuning of the older section.

Using these age constraints, we then tuned this section of

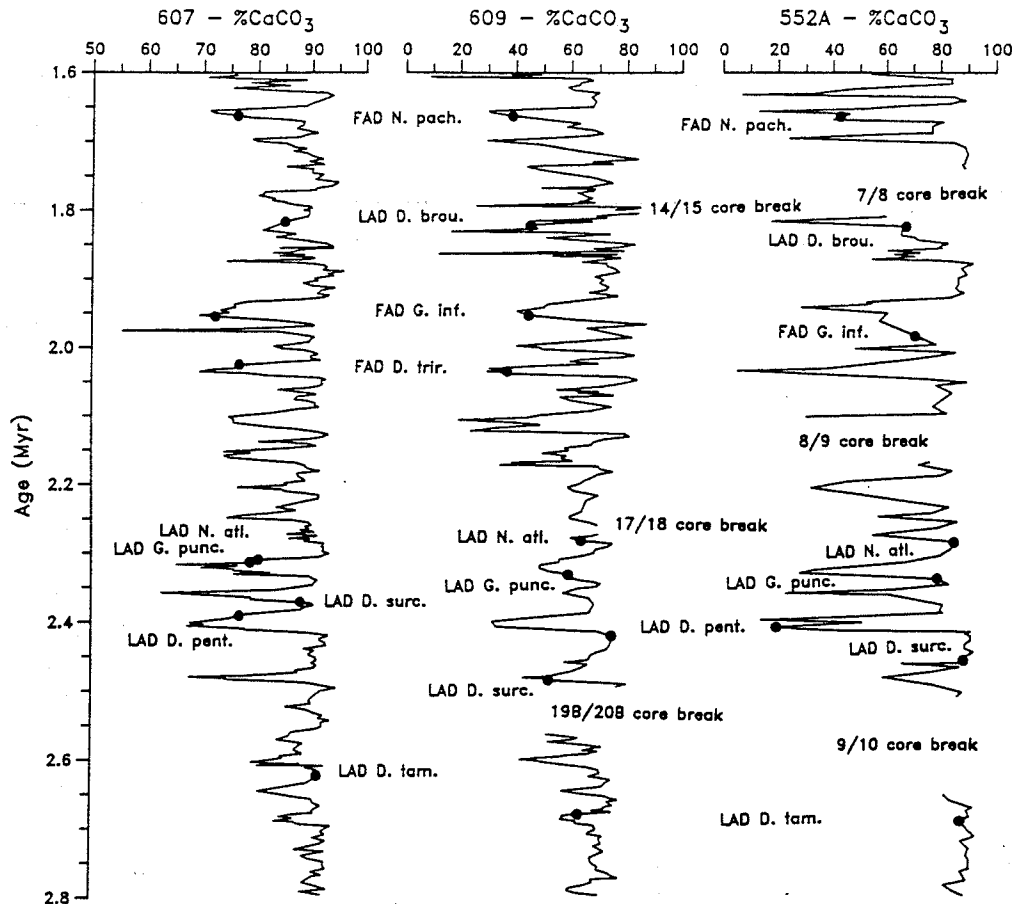


Fig. 10. Records of percent  $\text{CaCO}_3$  from site 609 and hole 552A correlated to the tuned percent  $\text{CaCO}_3$  record from site 607. All unspliced core breaks are identified and age ranges for biostratigraphic datums are summarized in Table 5. Datum abbreviations are: pach., *pachyderma* (s.) acme; brou., *brouweri*; inf., *inflata*; trir., *triradiatus* acme; atl., *atlantica*; punc., *puncticulata*; pent., *pentaradiatus*; surc., *surculus*; and tam., *tamalis*.

~7 cm/kyr. This interval of low sedimentation rates may have been caused by enhanced dissolution or by increased winnowing and erosion by bottom currents; it does not appear to have been the result of the coring disturbances that were so prevalent over this interval at site 609. However, it is apparent that a significant amount of sediment is missing at the unspliced 19B/20B core break. By correlation to site 607, we estimate that ~40 kyr has been missed across this core break.

Other unspliced core breaks can be similarly assessed with respect to site 607. The 14/15 break at hole 609 does not appear to be missing a significant amount of sediment. We have, however, modified the carbonate data already published [Ruddiman et al., 1986c] by deleting the first data point at the top of core 15 (609-15-1-0.75 cm). We removed this prominent carbonate low because of visual indications of downcore reworking. The other unspliced core break, between cores 17 and 18, does not appear to be missing more than 10 kyr of sediment.

At hole 552A, significant amounts of sediment are missing at all three core breaks. Inspection of Figure 11 indicates that ~60 kyr (stages 69 and 70) is missing at the 7/8

core break, ~65 kyr (stages 86-88) is missing at the 8/9 core break, and ~130 kyr (stages 107-113) is missing at the 9/10 core break.

#### Revised Ages of Magnetic Datums

Using the time scales developed for sites 607 and 609, we can determine new ages for the magnetic reversal datums listed in Table 3. Assuming that we have correctly mapped the climate signal into the orbital record during the tuning process, the new "tuned" ages should be more accurate than the radiometric ages, which have a stated error of 2%, or ~30 kyr, at the top of the Pliocene. By contrast, the error in absolute age of the orbital calculations is only about 5 kyr at 1.6 Ma [Berger, 1984]. (Uncertainty in the actual lag of the climate response after orbital forcing could also result in a few thousand year error.) In Table 8 we have listed the magnetic datums with the revised ages determined at each site. At site 607, estimated ages for the top of the Olduvai (1.65 Ma) and the Matuyama/Gauss boundary (2.48 Ma) both fall within 1% of the radiometric estimate. The tuned age for the bottom of the Olduvai (1.82 Ma) differs by about 3% from the

TABLE 8. Comparison of Published Ages of Magnetic Reversals Against Ages Derived Using TP607 Time Scale

Magnetic Reversal	Ages, Ma			
	Published	Composite Site 607	Composite Site 609	Site 552A
Top Olduvai	1.66 <sup>a</sup>	1.653	1.630-1.638	1.643-1.652
Bottom Olduvai	1.88 <sup>a</sup>	1.821-1.826	1.806-1.812	1.731-1.858
Top Reunion	2.01 <sup>b</sup>	---	1.982-2.003	1.881-1.889
Bottom Reunion	2.04 <sup>b</sup>	---	2.018-2.021	1.893-1.900
Matuyama/Gauss	2.48 <sup>b</sup>	2.481-2.486	2.460-2.475	2.457-2.466

<sup>a</sup> Berggren et al. [1986].

<sup>b</sup> Mankinen and Dalrymple [1979].

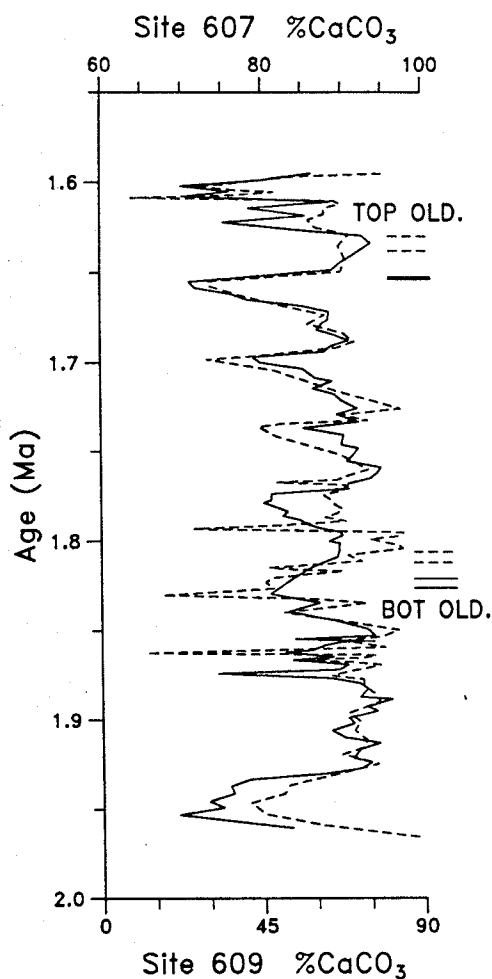


Fig. 12. Superposition of correlated percent  $\text{CaCO}_3$  records from 607 (solid line) and 609 (dashed line) for the interval from 1.60 to 1.95 Ma, showing position of the Olduvai magnetic subchron at each site. Width of uncertainty in the placement of reversals is indicated at right. In both cases, the position of the reversal in 609 falls later than in 607.

Thus, it appears that the maximum attainable accuracy in dating, even if our assumptions about the tuning methods are correct, is about 1%, or ~15 kyr. On the basis of our site 607 results (Table 8), we propose an age of 1.65 Ma for the top of the Olduvai (see also Ruddiman et al. [1986a; this issue]), 1.82 Ma for the bottom of the Olduvai, and 2.48 Ma for the Matuyama/Gauss boundary. Results from site 609 suggest that the Reunion event lasted from ~1.99 to 2.02 Ma. Because the Reunion event identified at hole 552A occurs much closer to the lower Olduvai reversal and dates about 100 kyr younger than at hole 609, we believe this to be a separate reversal, possibly equivalent to the minor event discovered at site 607 (Figure 3). Carbonate and biostratigraphic correlations between these two sites (Figure 10) support this conclusion.

#### Revised Ages of Biostratigraphic Datums

The foraminiferal and nannofossil datums listed in Tables 4 and 5 are plotted in Figure 10. The first abundant appearance of sinistrally coiled *Neogloboquadrina pachyderma* occurs at all three sites (607, 609, and 552A) within stage 64. This datum thus appears synchronous from 42° to 56°N latitude and dates at 1.66 Ma, within the age range proposed by Weaver and Clement [1986]. The first appearance datum (FAD) of *Globorotalia inflata* (d'Orbigny) is found within stage 78 at sites 607 and 609 but may fall slightly earlier at 552A. This event is dated at 1.96 Ma, ~100 kyr younger than the age proposed by Weaver and Clement [1986].

The last appearance datum (LAD) of *Neogloboquadrina atlantica* falls on the transition between stages 95 and 96 at site 607, on the stage 94-95 transition at site 609, and within stage 95 at site 552A. Our estimated age of 2.28-2.31 Ma is in agreement with that proposed by Weaver and Clement [1986]. The LAD of *Globorotalia puncticulata*, not dated by Weaver and Clement [1986], falls within stage 96 at site 607, on the 96/97 boundary at site 609, and within stage 97 at site 552A. This datum appears to be time transgressive, disappearing first at the more northern sites, and dates from 2.31 to 2.35 Ma. Unlike *G. puncticulata*, which has a subtropical/transitional affinity [Kennett and Srinivasan, 1983], *N. atlantica*, a polar/subpolar species [Poore, 1981], disappears earliest at the most southern site.

Of the nannofossil datums, *Discoaster brouweri* (LAD) falls within stage 72 at all three sites, and *Discoaster triradiatus* acme (FAD) falls within stage 82 at sites 607 and 609 (this datum was not identified at site 552). These events are dated at 1.83 Ma and 2.03 Ma, respectively, ~50 kyr

the top. Thus, core data from both the North Atlantic and Pacific Oceans support our 60,000-year revision to the age of the lower Olduvai.

The presently accepted estimate of the age of the Olduvai originally came from Klitgord et al. [1975] and was later corrected for a decay constant change by Mankinen and Dalrymple [1979]. Klitgord et al. [1975] used the relative length of seafloor magnetic anomalies along six East Pacific Rise tracks to calculate the age and length of the Olduvai subchron. Like Opdyke and Foster [1970], they interpolated between the radiometrically dated boundaries of the Matuyama Chron, but instead of assuming constant sedimentation rates, they assumed constant seafloor spreading rates. It is unclear why two such similar methods should give such different estimates for the length of the Olduvai. Possibly, the short magnetic event we discovered at sites 607, 609, and 611 (Figure 3) has blurred the marine magnetic anomaly record, making the Olduvai appear longer than it really is. At site 607, this event is ~10 kyr in duration and was identified ~100 cm (or 20 kyr) below the bottom of the Olduvai.

Other data which bear on this question are radiometric measurements from Olduvai Gorge and other sites, summarized and adjusted to new decay constants by Mankinen and Dalrymple [1979]. Anorthoclase samples from Olduvai Gorge give ages of 1.79 and 1.87 Ma for normally magnetized beds. However, a reversely magnetized bed in Madeira was also dated at 1.79 Ma. Of these three values, only the 1.79-Ma date from Olduvai Gorge would be in agreement with the changes proposed here. Yet, the analytic errors on these numbers (2% or ~40 kyr) are almost as great as the difference in ages we are proposing and, hence, cannot constrain our time scale estimates.

Our results, combined with those from other deep-sea cores, suggest that a significant reduction in the length of the Olduvai subchron may be required. Marine magnetic anomaly data from geographically widespread areas should be examined, given the limited geographic nature of the Klitgord et al. [1975] study. We propose that the Olduvai subchron dates from 1.65 to 1.82 Ma, our tuned estimate from site 607. These values are nearly identical to ages of 1.64-1.82 Ma obtained by Pisias and Moore [1981], who orbitally tuned the low-resolution planktonic  $\delta^{18}\text{O}$  record from V28-239.

## RESULTS

### Oxygen Isotopes

The oxygen isotope data presented in Figure 6 constitute the most detailed record of the initiation of northern hemisphere glaciation yet obtained. This record, slightly over 1 million years in length, is characterized by four distinctive intervals. In the first, from 2.75 to 2.42 Ma (stages 116-101), the  $\delta^{18}\text{O}$  signal is characterized by eight 41-kyr cycles which vary in amplitude from ~0.4 to 1.0‰. These cycles gradually increase in amplitude from 2.75 to 2.60 Ma, are of approximately constant amplitude (~1.0‰) between 2.60 and 2.48 Ma, and then abruptly fall in amplitude (to ~0.4‰) for one cycle at 2.44 Ma.

Within this interval (2.75-2.42 Ma), small amounts of ice-rafted debris (IRD) are found at sites 607, 609, and 552A [Shackleton et al., 1984]. At site 609, trace amounts were identified within glacial stages 110 and 112, and at site 607, IRD was found within stage 106. Thus, physical evidence points to the presence of continental ice sheets, most likely in North America, from at least 2.65 Ma. These ice sheets were

large enough, and North Atlantic sea surface temperatures (SSTs) were cold enough, to allow penetration of icebergs to 40°N, significantly further south than such ice travels today.

The second interval, between 2.42 and 2.30 Ma (stages 101-95), is characterized by three large isotope events which fall ~41 kyr apart (Figure 6). These events have an amplitude of 1.0-1.2‰, roughly two thirds the amplitude of the last glacial/interglacial cycle. Significant amounts of ice-rafted material are found at both sites 552A and 609 during these events [Shackleton et al., 1984; Raymo et al., 1986], and lesser amounts of IRD are found at site 607. Because it is associated with the first episode of large-scale ice-rafting in the North Atlantic, the glacial at 2.40 Ma (stage 100) is usually considered to mark the onset of significant northern hemisphere glaciation [Backman, 1979; Shackleton et al., 1984].

In Figure 11, the hole 552A  $\delta^{18}\text{O}$  signal has a much higher amplitude than 607 over this critical interval, indicating ice volume changes equivalent to those of the late Pleistocene [Shackleton et al., 1984]. However, Keigwin [1986], whose  $\delta^{18}\text{O}$  record from Site 606 had an amplitude similar to site 607, proposed that the 552A record may be biased by species disequilibrium effects. He showed that species offsets for *G. subglobosa*, the primary species used in this section of 552A, were not constant over this time interval. A reanalysis of the 552A record using only *Cibicidoides* species [Curry and Miller, 1989] supports this suggestion. Their *Cibicidoides* data show  $\delta^{18}\text{O}$  amplitudes similar to those observed at sites 607 and 606.

These three large events, centered at 2.40, 2.36, and 2.32 Ma (Table 7), did not herald a permanent increase in the amplitude of the oxygen isotope signal. Between 2.30 and 2.11 Ma (stages 95-86), the  $\delta^{18}\text{O}$  record again is characterized by low-amplitude variations, 0.5 to 1.0‰, which are as small as, or smaller than, those which occurred prior to 2.40 Ma. Similar decreases in  $\delta^{18}\text{O}$  amplitude are observed at sites 606 [Keigwin, 1986], 552A [Shackleton et al., 1984; Curry and Miller, 1989], and, to a much lesser extent, 665 [Curry and Miller, 1989]. No IRD was detected at sites 607 or 609 from stages 89 through 95. Within glacial stages 86 and 88, IRD was detected at site 609 but not at site 607. Small amounts of IRD are found at site 552A throughout this interval. Thus, following the large glaciation at 2.32 Ma (stage 96), it was almost 280 kyr before ice-rafting again reached the latitude of site 607.

Subsequent to 2.11 Ma, the amplitude of the  $\delta^{18}\text{O}$  signal again increases, varying between ~3.3 and 4.2‰ (range of ~0.9‰). However, within this interval, there are also numerous small events (amplitude <0.5‰) which seem to be modulated by the 23-kyr and 96-kyr periods of precession and eccentricity (as discussed in the time scale section). This interval contrasts with the following interval, between 1.5 and 1.1 Ma [see Ruddiman et al., this issue], where  $\delta^{18}\text{O}$  variations have approximately the same amplitude yet show no strong indications of eccentricity or precession.

Taken as a whole, the  $\delta^{18}\text{O}$  record presented in Figure 6 shows that the onset of northern hemisphere glaciation was not a simple unidirectional increase in ice sheet size. Although the interglacial isotopic values appear to be gradually becoming heavier, the glacial values fluctuate significantly between times of apparently large ice volume (e.g., stages 96, 98, and 100) and times of very minor ice volume (e.g., stages 90, 92, and 94). That these  $\delta^{18}\text{O}$  variations represent, in large part, variations in northern

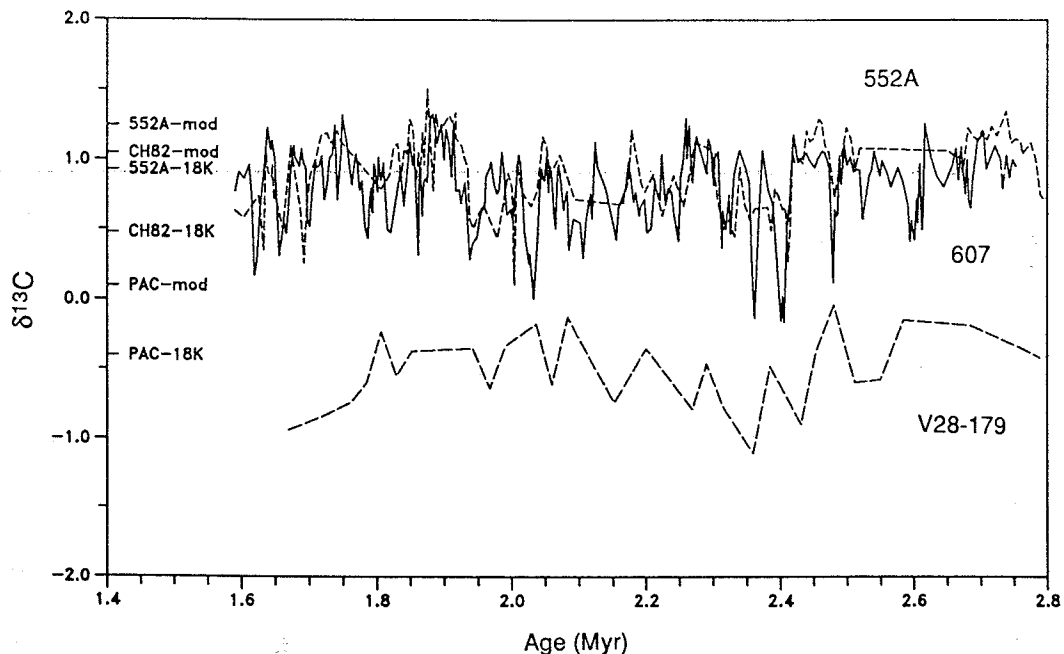


Fig. 13. Records of  $\delta^{13}\text{C}$  from 552A (short-dashed line) [from Shackleton and Hall, 1984], 607 (solid line), and V28-179 (long-dashed line) [from Shackleton and Opdyke, 1977]. V28-179 is located in the central equatorial Pacific Ocean at  $4^\circ\text{N}$ ,  $139^\circ\text{W}$  (4509 m). Modern and 18-kyr  $\delta^{13}\text{C}$  values for the Atlantic sites are indicated at right (CHN82-24-4, abbreviated CH82, was used to represent site 607, as no measurements were made at the top of this core). Average modern and 18-kyr values were used for the deep Pacific Ocean. All data were adjusted for species offsets. The 552A record, which is based on a number of benthic species, compares very favorably with the *Cibicidoides*  $\delta^{13}\text{C}$  record generated from this core by Curry and Miller [1989].

levels. Relative to the amplitude of the  $\delta^{18}\text{O}$  signal, 607 and 552A exhibit significantly larger variations in  $\delta^{13}\text{C}$  in the late Pliocene than in the late Quaternary. At 2.40 Ma, when  $\delta^{18}\text{O}$  values suggest only half the ice sheet growth of the last glacial maximum,  $\delta^{13}\text{C}$  values at site 607 reach  $-0.15\text{‰}$ , almost  $0.5\text{‰}$  more negative than at 18 kyr B.P. At site 552A,  $\delta^{13}\text{C}$  values are almost  $0.6\text{‰}$  more negative than 18-kyr values (Figure 13). In general, throughout the 1.2 m.y. length of these records, the amplitudes of the  $\delta^{13}\text{C}$  signals are very large, given the relatively modest ice volume changes suggested by the  $\delta^{18}\text{O}$  record.

We know that NADW was being formed throughout the late Pliocene because North Atlantic cores are always significantly more enriched in  $^{13}\text{C}$  than are Pacific records [Shackleton et al., 1984] (Figure 13). Yet, it is difficult to understand the high amplitude of the 552A and 607  $\delta^{13}\text{C}$  signals using the oceanographic model developed for the late Pleistocene [e.g., Boyle and Keigwin, 1985/1986; Oppo and Fairbanks, 1987]. In this model, the depletion of Atlantic  $\delta^{13}\text{C}$  values during glacials is caused both by the increased influence of SOW relative to NADW and by a decrease in the size of the terrestrial carbon reservoir. Thus, for late Pliocene glacial  $\delta^{13}\text{C}$  values to be more negative, either (1) larger relative reductions in NADW production must occur or (2) there must be larger glacial-interglacial transfers of  $^{12}\text{C}$  between the continents and oceans. A third possibility, that there were significant increases in the preformed nutrient

content of NADW during glacials, also cannot be ruled out.

If the relatively lighter  $\delta^{13}\text{C}$  values observed in the late Pliocene were due to greater glacial-interglacial transfers between carbon reservoirs, then all deep-sea  $\delta^{13}\text{C}$  records should show a larger-amplitude signal relative to the late Pleistocene. Indeed, Pacific  $\delta^{13}\text{C}$  values from this time are also significantly lighter during glacials than is observed during the late Pleistocene;  $\delta^{13}\text{C}$  values from V28-179 (Figure 13) and from site 677 (N. J. Shackleton, personal communication, 1988) are often less than  $-0.5\text{‰}$  during the late Pliocene, and the glacial-interglacial amplitudes of the  $\delta^{13}\text{C}$  signals at these sites are also larger than is observed in the late Pleistocene. Thus, relatively more negative glacial  $\delta^{13}\text{C}$  values seem to characterize both oceans, indicating that glacial-interglacial changes in the global  $\delta^{13}\text{C}$  reservoir may be the primary factor driving the larger-amplitude  $\delta^{13}\text{C}$  signals observed in the late Pliocene. However, we cannot rule out the possibility that large deepwater circulation changes are recorded by the Pacific  $\delta^{13}\text{C}$  records. In addition, because the  $\delta^{13}\text{C}$  gradient between site 607 and site 552 is generally larger during glaciations, it does appear that some glacial suppression of NADW was also occurring at this time (e.g., during stages 104, 100, 98, and 82). Until more  $\delta^{13}\text{C}$  and cadmium records are collected from many areas of the ocean, we will not be able to determine with certainty the relative influence of these effects on the  $\delta^{13}\text{C}$  records at these sites.

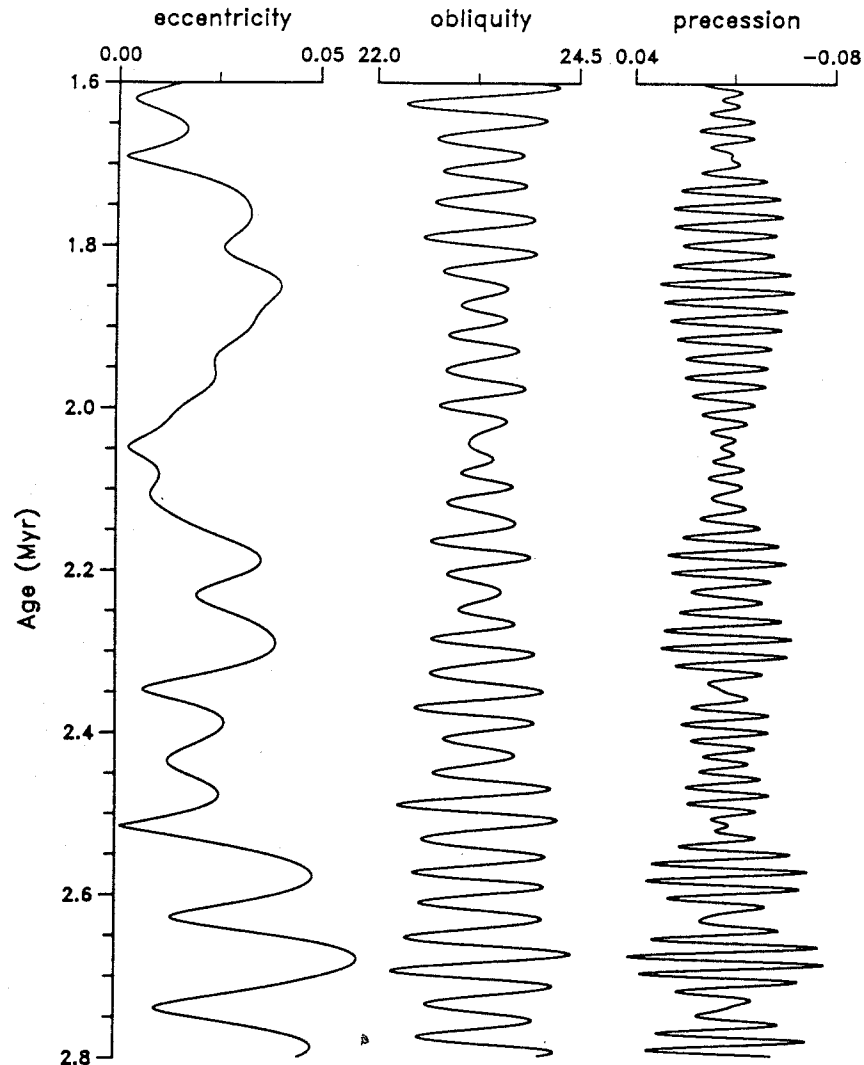


Fig. 16. Variations in eccentricity, obliquity, and precession derived by Berger [1976] for the interval 1.6-2.8 Ma.

3.6 and 2.0 Ma, also appear to vary at the 400 kyr eccentricity period [Backman and Pestiaux, 1986].

Such a correlation between the orbital forcing and the climate response is not, however, observed for the 96-kyr band. At the time of the strongest 96-kyr response, between 1.85 and 2.10 Ma, Figure 16 shows that the 96-kyr component of eccentricity almost entirely disappears. Thus, it appears that late Pliocene climate variations at the 96-kyr frequency are, in a sense, decoupled from the orbital forcing and, indeed, may not be related to orbital variations at all [Oerlemans, 1980; Saltzman and Sutera, 1984; Saltzman et al., 1984].

The presence of 100-kyr power in the late Pliocene is thus relevant to the evaluation of existing climate theories. The dominance of the 100-kyr component in the late Pleistocene has been ascribed to nonlinear feedbacks caused by different time constants for the decay and growth of ice sheets [Imbrie and Imbrie, 1980]. The larger the asymmetry, the greater the low-frequency response that results. Within the late Pliocene

interval, stages 78-86 do appear to exhibit the beginnings of this asymmetry, with deglaciations at 2.10 and 2.02 Ma apparently being more rapid than the following periods of ice sheet growth (Figure 6).

However, it is the cause of the asymmetry, or differing time constants, that is at question. Piasis and Moore [1981] have proposed that gradual erosion of continental areas under the ice sheets have allowed the late Pleistocene transition to marine-based ice sheets and, hence, rapid rates of glacial decay. Yet, a bedrock erosion mechanism would predict a one-way evolution of the ice sheet system and could not explain the absence of 100-kyr power between 1.5 and 1.1 Ma [Ruddiman et al., 1986a; this issue]. Likewise, the  $\delta^{18}\text{O}$  record indicates that the ice sheets around 2.1 Ma are not significantly larger than those which occur solely at the 41-kyr frequency between 1.0 and 1.5 Ma. Therefore, nonlinearities arising from the degree of bedrock depression and rebound [Oerlemans, 1980; Birchfield and Grumbine, 1985] should not be different at these times. In summary, progressive bedrock erosion and ice sheet

TABLE A1. (continued)

DSDP Sample Identification			Composite Depth, m	Age Ma <sup>a</sup>	CaCO <sub>3</sub> %	δ <sup>18</sup> O ‰	δ <sup>13</sup> C ‰	Species Code <sup>b</sup>
Hole	Core-section	Depth, cm						
607A	9-5	15.0	72.44	1.6223	75.3	3.84	-0.63	U
607A	9-5	30.0	72.60	1.6264	84.4	4.13	-0.28	U
607	9-1	1.0	72.71	1.6295	92.6			
607	9-1	16.0	72.85	1.6338	93.8	2.73	0.99	C
607	9-1	31.0	73.00	1.6375		2.76	1.23	C
607	9-1	53.0	73.22	1.6426	90.7	2.90	1.07	C
607	9-1	61.0	73.31	1.6445	90.0	2.91	1.14	C
607	9-1	78.0	73.47	1.6485	88.9	3.12	1.00	C
607	9-1	106.0	73.75	1.6551	71.1	3.35	0.31	C
607	9-1	121.0	73.90	1.6584	71.8			
607	9-1	136.0	74.06	1.6618	76.3	4.00	-0.34	U
607	9-2	1.0	74.21	1.6651	78.4	4.03	-0.43	U
607	9-2	16.0	74.35	1.6684	85.2	3.89	-0.25	U
607	9-2	31.0	74.50	1.6717	88.5	3.64	0.02	U
607	9-2	53.0	74.72	1.6764	88.4	2.68	1.10	C
607	9-2	61.0	74.81	1.6781	87.7	2.82	1.02	C
607	9-2	78.0	74.97	1.6817	87.0	3.05	0.98	C
607	9-2	91.0	75.10	1.6844	89.1	2.95	0.95	C
607	9-2	106.0	75.25	1.6875	91.0	2.82	1.08	C
607	9-2	121.0	75.40	1.6906	88.8	2.94	0.97	C
607	9-2	136.0	75.56	1.6937	87.9	2.81	0.95	C
607	9-3	1.0	75.71	1.6968	79.0	3.13	0.56	C
607	9-3	1.0	75.71	1.6968		2.91	0.55	C
607	9-3	16.0	75.85	1.6999	79.9	4.33	-0.38	U
607	9-3	16.0	75.85	1.6999		3.66	0.52	C
607	9-3	31.0	76.00	1.7034	85.2	3.83	0.00	U
607	9-3	31.0	76.00	1.7034		3.26	0.62	C
607	9-3	53.0	76.22	1.7085	86.8	3.01	1.05	C
607	9-3	53.0	76.22	1.7085		3.55	0.02	U
607	9-3	61.0	76.31	1.7104	88.9	3.66	-0.01	U
607	9-3	61.0	76.31	1.7104		2.94	0.98	C
607	9-3	78.0	76.47	1.7145	86.5	3.62	0.02	U
607	9-3	78.0	76.47	1.7145		3.01	1.01	C
607	9-3	91.0	76.60	1.7177	89.1	2.82	1.03	C
607	9-3	106.0	76.75	1.7214	90.0	2.94	0.71	C
607	9-3	123.0	76.92	1.7257	92.0	3.36	0.72	C
607	9-3	123.0	76.92	1.7257		3.13	0.91	C
607	9-3	136.0	77.06	1.7290	89.4	2.86	0.91	C
607	9-3	136.0	77.06	1.7290		3.67	0.24	U
607	9-3	136.0	77.06	1.7290		2.92	0.98	C
607	9-4	3.0	77.22	1.7333	92.2	3.56	0.14	U
607	9-4	16.0	77.35	1.7367	85.2	2.83	1.25	C
607	9-4	31.0	77.50	1.7406	90.3	2.96	0.71	C
607	9-4	53.0	77.72	1.7462	90.0	2.85	1.05	C
607	9-4	61.0	77.81	1.7482	92.1	3.05	1.32	C
607	9-4	78.0	77.97	1.7524	91.4			
607	9-4	91.0	78.10	1.7556	90.6	2.93	1.10	C
607	9-4	106.0	78.25	1.7591	94.9	2.72	0.93	C
607	9-4	121.0	78.40	1.7623	94.4	3.02	0.82	C
607	9-4	136.0	78.56	1.7653	93.5	2.82	0.94	C
607	9-5	1.0	78.71	1.7682	90.8	3.16	1.04	C
607	9-5	16.0	78.85	1.7709	90.8	3.30	0.96	C
607	9-5	31.0	79.00	1.7736	81.2	3.53	0.78	C
607	9-5	31.0	79.00	1.7736		3.32	0.78	C
607	9-5	53.0	79.22	1.7775	81.1	3.50	0.85	C
607	9-5	61.0	79.31	1.7788	80.2	3.29	0.71	C
607	9-5	78.0	79.47	1.7816	82.1	3.52	0.52	C
607	9-5	91.0	79.60	1.7836	83.3			

TABLE A1. (continued)

DSDP Sample Identification			Composite Depth, m	Age Ma <sup>a</sup>	CaCO <sub>3</sub> %	δ <sup>18</sup> O ‰	δ <sup>13</sup> C ‰	Species Code <sup>b</sup>
Hole	Core-section	Depth, cm						
607	10-3	136.0	86.89	1.9413	76.2	3.60	0.40	C
607	10-4	3.0	87.06	1.9458	73.1	3.54	0.45	C
607	10-4	16.0	87.19	1.9493	74.9	3.42	0.45	C
607	10-4	31.0	87.35	1.9533	69.4	3.39	0.62	C
607	10-4	53.0	87.56	1.9591	80.4	3.13	0.68	C
607	10-4	59.0	87.63	1.9607	83.5	3.13	0.88	C
607	10-4	78.0	87.81	1.9657	89.7	3.03	0.94	C
607	10-4	89.0	87.92	1.9686	90.6	2.86	0.99	C
607	10-4	97.5	88.01	1.9708	84.7			
607	10-4	106.0	88.10	1.9730	76.3	3.05	0.83	C
607	10-4	115.5	88.19	1.9754	55.6			
607	10-4	123.0	88.26	1.9773	83.8	2.97	0.76	C
607	10-4	136.0	88.39	1.9805	87.1	3.07	0.79	C
607	10-5	3.0	88.56	1.9847	90.7	2.85	1.06	C
607	10-5	16.0	88.69	1.9878	90.1	2.69	0.93	C
607	10-5	35.0	88.88	1.9922	89.6	2.73	0.61	C
607	10-5	53.0	89.06	1.9962	85.7	2.82	0.63	C
607	10-5	61.0	89.14	1.9979	83.2	2.73	0.65	C
607	10-5	78.0	89.31	2.0015	84.6	3.25	0.57	C
607	10-5	91.0	89.44	2.0041	88.7	3.10	0.70	C
607	10-5	106.0	89.60	2.0070	90.5			
607	10-5	121.0	89.74	2.0099	91.3	2.65	1.04	C
607	10-5	136.0	89.89	2.0127	89.9	2.52	0.98	C
607	10-6	1.0	90.04	2.0156	90.0	2.71	0.78	C
607	10-6	16.0	90.19	2.0186	91.8	2.90	0.49	C
607	10-6	31.0	90.35	2.0214	84.7			
607	10-6	53.0	90.56	2.0255	77.0	3.54	0.26	C
607	10-6	59.0	90.63	2.0266	77.0	3.72	0.33	C
607	10-6	78.0	90.81	2.0301	76.0			
607	10-6	89.0	90.92	2.0321	71.1	3.49	0.01	C
607	10-6	106.0	91.10	2.0353	69.6			
607	10-6	119.0	91.22	2.0377	78.1	3.22	0.42	C
607	10-6	136.0	91.39	2.0409	81.8	3.20	0.76	C
607	10-7	3.0	91.56	2.0441	91.4	2.90	0.94	C
607	10-7	16.0	91.69	2.0467	92.8	2.95	0.87	C
607	10-7	27.0	91.81	2.0488	92.0	2.79	0.85	C
607A	11-4	15.0	91.94	2.0514	92.1	2.75	1.03	C
607A	11-4	31.0	92.10	2.0540	92.3	2.95	0.77	C
607A	11-4	45.0	92.24	2.0563	91.4	2.95	0.96	C
607A	11-4	61.0	92.40	2.0591	89.7	2.98	0.87	C
607A	11-4	75.0	92.54	2.0615	83.9	3.11	0.64	C
607A	11-4	91.0	92.70	2.0644	86.6	3.08	0.51	C
607	11-1	5.0	92.85	2.0670	89.8	2.74	0.89	C
607	11-1	16.0	92.95	2.0691	91.0	2.97	0.97	C
607	11-1	31.0	93.10	2.0720	87.6	2.91	0.87	C
607	11-1	53.0	93.32	2.0764	87.0	2.90	0.64	C
607	11-1	61.0	93.40	2.0780	89.1	2.79	0.70	C
607	11-1	78.0	93.57	2.0815	90.9	2.75	0.78	C
607	11-1	91.0	93.70	2.0843	90.8	2.88	0.36	C
607	11-1	106.0	93.85	2.0877	91.6			
607	11-1	121.0	94.00	2.0911	87.0	2.54	0.58	C
607	11-1	136.0	94.15	2.0963	82.5			
607	11-2	1.0	94.31	2.1015	74.9	2.97	0.55	C
607	11-2	16.0	94.45	2.1058	75.9	3.48	0.30	C
607	11-2	31.0	94.60	2.1104	75.8	3.06	0.59	C
607	11-2	53.0	94.82	2.1170	82.9	3.08	0.76	C
607	11-2	61.0	94.90	2.1193	86.7	2.92	0.58	C
607	11-2	78.0	95.07	2.1240	91.4	2.67	1.13	C

TABLE A1. (continued)

DSDP Sample Identification			Composite Depth, m	Age Ma <sup>a</sup>	CaCO <sub>3</sub> %	$\delta^{18}\text{O}$ ‰	$\delta^{13}\text{C}$ ‰	Species Code <sup>b</sup>
Hole	Core-section	Depth, cm						
607A	12-4	61.0	102.93	2.3007	93.5	2.76	0.82	C
607A	12-4	75.0	103.07	2.3031	92.7	2.58	1.05	C
607	12-1	5.0	103.24	2.3057	91.6	2.74	1.03	C
607	12-1	16.0	103.35	2.3075	88.0	2.89	1.06	C
607	12-1	31.0	103.49	2.3099	80.3	3.11	0.77	C
607	12-1	53.0	103.71	2.3133	79.4	3.55	0.37	C
607	12-1	61.0	103.79	2.3145	78.2	3.74	0.64	C
607	12-1	78.0	103.96	2.3171	65.5	3.52	0.57	C
607	12-1	91.0	104.10	2.3191	76.6	3.56	0.50	C
607	12-1	106.0	104.24	2.3214	69.9			
607	12-1	121.0	104.39	2.3237	76.0	3.29	0.75	C
607	12-1	136.0	104.54	2.3261	75.9	3.10	0.47	C
607	12-2	1.0	104.69	2.3286	82.6			
607	12-2	16.0	104.85	2.3311	75.9	3.07	0.89	C
607	12-2	31.0	104.99	2.3339	89.7			
607	12-2	53.0	105.21	2.3380	90.7	2.62	1.05	C
607	12-2	61.0	105.29	2.3396	91.3	2.59	1.07	C
607	12-2	78.0	105.46	2.3435	90.8			
607	12-2	91.0	105.60	2.3465	90.6			
607	12-2	106.0	105.74	2.3499	87.4	2.84	0.92	C
607	12-2	121.0	105.89	2.3537	83.7	3.35	0.83	C
607	12-2	136.0	106.04	2.3577	62.6	3.49	0.20	C
607	12-3	1.0	106.19	2.3615	72.2	3.51	-0.13	C
607	12-3	16.0	106.35	2.3646	79.1			
607	12-3	31.0	106.49	2.3677	79.0	3.39	0.55	C
607	12-3	53.0	106.71	2.3719	88.2	3.07	0.92	C
607	12-3	61.0	106.79	2.3733	90.2	3.07	1.07	C
607	12-3	78.0	106.96	2.3761	90.6			
607	12-3	89.0	107.07	2.3779	89.2	2.81	0.92	C
607	12-3	106.0	107.24	2.3823	88.3	2.64	0.78	C
607	12-3	121.0	107.39	2.3891	77.6	3.27	0.68	C
607	12-3	136.0	107.54	2.3950	74.9			
607	12-4	1.0	107.69	2.4009	67.9	3.78	-0.15	C
607	12-4	16.0	107.85	2.4035	70.4	3.67	0.03	C
607	12-4	29.0	107.97	2.4058	67.3	3.66	-0.16	C
607	12-4	53.0	108.21	2.4098	77.9	3.44	0.53	C
607	12-4	61.0	108.29	2.4112	77.7	3.52	0.56	C
607	12-4	78.0	108.46	2.4142	85.5	3.15	0.72	C
607	12-4	89.0	108.57	2.4163	89.7	2.92	0.90	C
607	12-4	106.0	108.74	2.4196	93.4	2.71	1.18	C
607	12-4	121.0	108.89	2.4220	92.9			
607	12-4	136.0	109.04	2.4243	91.8			
607	12-5	1.0	109.19	2.4266	91.8	2.74	0.98	C
607	12-5	16.0	109.35	2.4302	92.9			
607	12-5	32.5	109.51	2.4341	93.0			
607	12-5	53.0	109.71	2.4390	88.9	2.87	1.05	C
607	12-5	61.0	109.79	2.4416	90.8	2.97	0.99	C
607	12-5	78.0	109.96	2.4477	89.7	2.73	0.99	C
607	12-5	91.0	110.10	2.4519	91.1	2.64	0.94	C
607	12-5	106.0	110.24	2.4560	91.3	2.71	1.00	C
607	12-5	121.0	110.39	2.4595	90.3			
607	12-5	136.0	110.54	2.4629	91.3	2.59	1.06	C
607	12-6	1.0	110.69	2.4669	90.9	2.69	1.05	C
607	12-6	16.0	110.85	2.4704	87.3	2.67	1.00	C
607	12-6	31.0	110.99	2.4736	87.8	2.95	0.94	C
607	12-6	53.0	111.21	2.4780	78.0	2.97	0.33	C
607	12-6	61.0	111.29	2.4796	67.7	3.38	0.12	C

TABLE A1. (continued)

DSDP Sample Identification			Composite Depth, m	Age Ma <sup>a</sup>	CaCO <sub>3</sub> %	$\delta^{18}\text{O}$ ‰	$\delta^{13}\text{C}$ ‰	Species Code <sup>b</sup>
Hole	Core-section	Depth, cm						
607	13-5	61.0	119.88	2.6898	87.1	2.97	0.93	C
607	13-5	78.0	120.06	2.6932	88.1	2.77	1.13	C
607	13-5	91.0	120.18	2.6961	94.0	2.66	1.13	C
607	13-5	106.0	120.33	2.7001	93.1			
607	13-5	121.0	120.49	2.7042	92.3	2.48	1.19	C
607	13-5	136.0	120.63	2.7082	93.1	2.48	0.93	C
607	13-6	1.0	120.78	2.7129	90.8			
607	13-6	16.0	120.93	2.7175	93.1			
607	13-6	29.0	121.06	2.7215	92.3	2.79	1.10	C
607	13-6	53.0	121.31	2.7298	87.4	2.89	1.00	C
607	13-6	61.0	121.38	2.7329	92.9	2.53	0.79	C
607	13-6	78.0	121.56	2.7391	88.8	2.68	1.03	C
607	13-6	91.0	121.68	2.7435	89.9	2.41	0.87	C
607	13-6	106.0	121.83	2.7483	92.9	2.63	1.00	C
607	13-6	106.0	121.83	2.7483		2.46	1.01	C
607	13-6	121.0	121.99	2.7530	92.8	2.43	0.95	C
607	13-6	136.0	122.13	2.7577	93.2			
607	13-7	1.0	122.28	2.7624	90.5			
607	13-7	16.0	122.43	2.7671	92.5			
607	13-7	21.0	122.49	2.7687	90.9			
607A	14-5	1.0	122.64	2.7737	89.8			
607A	14-5	15.0	122.78	2.7781	89.0			
607A	14-5	30.5	122.94	2.7829	91.5			
607	14-1	5.0	123.09	2.7876	93.4			
607	14-1	16.0	123.20	2.7911	88.6			
607	14-1	31.0	123.35	2.7958	92.3			
607	14-1	53.0	123.57	2.8027	91.1			
607	14-1	61.0	123.65	2.8052	92.7			
607	14-1	78.0	123.82	2.8105	91.7			
607	14-1	91.0	123.95	2.8146	97.1			

<sup>a</sup> Ages based on TP607 time scale.<sup>b</sup> C, *Cibicides*; U, *Uvigerina*. Isotope data not corrected for species offsets.TABLE A2. Percent CaCO<sub>3</sub> Data from Site 609

DSDP Sample Identification		Composite Depth, m	Age Ma <sup>a</sup>	CaCO <sub>3</sub> %
Hole	Core- section			
609	13-3	1.0	117.97	58.2
609	13-3	31.0	118.27	79.0
609	13-3	45.5	118.42	55.3
609	13-3	61.0	118.57	27.1
609	13-3	91.0	118.87	38.0
609	13-3	121.0	119.17	48.8
609	13-4	1.0	119.47	38.2
609	13-4	15.5	119.61	8.7
609	13-4	31.0	119.77	65.4
609	13-4	61.0	120.07	67.4
609	13-4	91.0	120.37	62.9
609	13-4	121.0	120.67	62.9
609	13-5	1.0	120.97	58.5
609	13-5	31.0	121.27	60.6
609	13-5	61.0	121.57	69.7
609	13-5	91.0	121.87	66.9

TABLE A2. (continued)

DSDP Sample Identification		Composite Depth, m	Age Ma <sup>a</sup>	CaCO <sub>3</sub> %
Hole	Core- section			
609	13-5	121.0	122.17	68.7
609	13-6	1.0	122.47	67.6
609	13-6	15.5	122.61	30.0
609	13-6	31.0	122.77	31.0
609	13-6	61.0	123.07	39.8
609	13-6	91.0	123.37	50.7
609B	14-2	121.0	123.67	63.0
609B	14-3	1.0	123.97	58.3
609B	14-3	31.0	124.27	68.2
609	14-1	5.0	124.57	71.2
609	14-1	31.0	124.83	66.1
609	14-1	61.0	125.13	47.1
609	14-1	75.5	125.27	29.8
609	14-1	91.0	125.43	48.7
609	14-1	121.0	125.73	65.7
609	14-2	1.0	126.03	84.0

TABLE A2. (continued)

DSDP Sample Identification					
Hole	Core-section	Depth, cm	Composite Depth, m	Age Ma <sup>a</sup>	CaCO <sub>3</sub> %
609	17-3	31.0	157.79	2.1339	72.3
609	17-3	61.0	158.10	2.1380	68.7
609	17-3	91.0	158.39	2.1421	67.9
609	17-3	121.0	158.69	2.1462	58.4
609	17-4	1.0	158.99	2.1502	59.8
609	17-4	31.0	159.29	2.1542	50.6
609	17-4	61.0	159.60	2.1582	59.1
609	17-4	91.0	159.89	2.1620	56.9
609	17-4	121.0	160.19	2.1659	61.2
609	17-4	134.5	160.33	2.1676	39.2
609	17-5	1.0	160.49	2.1697	47.9
609	17-5	15.5	160.64	2.1715	35.1
609	17-5	31.0	160.79	2.1735	70.3
609	17-5	61.0	161.10	2.1773	71.0
609	17-5	91.0	161.39	2.1812	75.6
609	17-5	121.0	161.69	2.1853	70.2
609	17-6	1.0	161.99	2.1895	68.1
609	17-6	31.0	162.29	2.1939	65.6
609	17-6	61.0	162.60	2.1985	63.8
609	17-6	91.0	162.89	2.2033	59.6
609	17-6	121.0	163.19	2.2094	61.8
609	17-7	1.0	163.49	2.2157	70.4
609	17-7	31.0	163.79	2.2235	66.2
609	18-1	31.0	164.39	2.2393	64.6
609	18-1	61.0	164.69	2.2459	60.5
609	18-1	91.0	164.99	2.2494	60.4
609	18-1	121.0	165.29	2.2525	63.8
609	18-2	5.0	165.63	2.2558	67.7
609	18-2	31.0	165.89	2.2582	69.1
609	18-2	46.0	166.04	2.2596	70.1
609B	19-1	1.0	167.39	2.2721	70.3
609B	19-1	31.0	167.69	2.2749	68.4
609B	19-1	61.0	167.99	2.2777	60.7
609B	19-1	91.0	168.29	2.2819	64.4
609B	19-1	121.0	168.60	2.2863	75.6
609B	19-2	1.0	168.89	2.2907	74.0
609B	19-2	31.0	169.19	2.2952	69.4
609B	19-2	61.0	169.49	2.2998	68.9
609B	19-2	91.0	169.79	2.3043	64.6
609B	19-2	121.0	170.10	2.3089	57.0
609B	19-3	1.0	170.39	2.3133	56.6
609B	19-3	31.0	170.69	2.3175	49.8
609B	19-3	61.0	170.99	2.3220	49.6
609B	19-3	91.0	171.29	2.3268	53.0
609B	19-3	121.0	171.60	2.3312	60.5
609B	19-4	1.0	171.89	2.3354	59.3
609B	19-4	31.0	172.19	2.3394	63.6
609B	19-4	61.0	172.49	2.3432	69.8
609B	19-4	76.0	172.64	2.3451	71.3
609B	19-4	91.0	172.79	2.3470	70.4
609B	19-4	106.0	172.94	2.3488	70.2
609B	19-4	121.0	173.10	2.3514	63.2
609B	19-4	136.0	173.24	2.3583	58.0
609B	19-5	1.0	173.39	2.3659	67.4
609B	19-5	16.0	173.54	2.3751	69.1
609B	19-5	31.0	173.69	2.3871	67.3
609B	19-5	46.0	173.85	2.3992	32.6
609B	19-5	61.8	174.00	2.4072	33.9

TABLE A2. (continued)

DSDP Sample Identification					
Hole	Core-section	Depth, cm	Composite Depth, m	Age Ma <sup>a</sup>	CaCO <sub>3</sub> %
609B	19-5	76.0	174.14	2.4144	70.4
609B	19-5	91.0	174.29	2.4218	75.9
609B	19-5	106.0	174.44	2.4346	74.8
609B	19-5	121.0	174.60	2.4402	73.7
609B	19-5	136.0	174.74	2.4446	70.1
609B	19-6	1.0	174.89	2.4485	67.9
609B	19-6	16.0	175.04	2.4522	67.7
609B	19-6	31.0	175.19	2.4556	66.9
609B	19-6	46.0	175.35	2.4588	58.7
609B	19-6	61.0	175.49	2.4619	66.8
609B	19-6	76.0	175.64	2.4649	65.8
609B	19-6	91.0	175.79	2.4719	61.5
609B	19-6	106.0	175.94	2.4795	52.5
609B	19-6	121.0	176.10	2.4814	43.8
609B	19-6	135.5	176.24	2.4831	53.8
609B	19-7	1.0	176.39	2.4848	52.3
609B	19-7	31.0	176.69	2.4909	80.8
609B	19-7	49.0	176.88	2.4946	77.4
609B	20-1	1.0	176.99	2.5632	52.3
609B	20-1	31.0	177.29	2.5687	63.7
609B	20-1	61.0	177.60	2.5714	61.2
609B	20-1	91.0	177.89	2.5741	53.2
609B	20-1	121.0	178.19	2.5768	60.5
609B	20-2	1.0	178.49	2.5794	67.4
609B	20-2	31.0	178.79	2.5820	72.0
609B	20-2	61.0	179.10	2.5846	67.6
609B	20-2	91.0	179.39	2.5866	65.4
609B	20-2	121.0	179.69	2.5884	70.7
609B	20-3	1.0	179.99	2.5902	68.5
609B	20-3	31.0	180.29	2.5920	67.4
609	20-2	31.0	180.60	2.5938	59.5
609	20-2	61.0	180.89	2.5957	56.5
609	20-2	75.5	181.04	2.5973	49.6
609	20-2	91.0	181.19	2.6000	43.0
609	20-2	105.5	181.34	2.6017	49.0
609	20-2	121.0	181.49	2.6036	51.2
609	20-3	1.0	181.79	2.6073	58.7
609	20-3	31.0	182.10	2.6113	66.6
609	20-3	61.0	182.39	2.6154	71.3
609	20-3	91.0	182.69	2.6198	71.7
609	20-3	121.0	182.99	2.6244	67.7
609	20-4	1.0	183.29	2.6293	75.5
609	20-4	31.0	183.60	2.6345	73.6
609	20-4	61.0	183.89	2.6397	72.1
609	20-4	91.0	184.19	2.6448	58.1
609	20-4	121.0	184.49	2.6475	61.7
609	20-5	1.0	184.79	2.6503	66.5
609	20-5	31.0	185.10	2.6531	73.4
609	20-5	61.0	185.39	2.6559	75.1
609	20-5	91.0	185.69	2.6587	78.0
609	20-5	121.0	185.99	2.6614	74.3
609	20-6	1.0	186.29	2.6640	75.3
609	20-6	31.0	186.60	2.6666	76.3
609B	21-1	61.0	186.89	2.6691	73.0
609B	21-1	91.0	187.19	2.6715	73.4
609B	21-1	121.0	187.49	2.6738	68.8
609B	21-2	1.0	187.79	2.6761	75.8
609B	21-2	31.0	188.10	2.6783	66.9

- southwest Pacific Ocean: Application of the graphic correlation method, *Paleoceanography*, 3, 209-222, 1988.
- Duplessy, J. C., N. J. Shackleton, R. G. Fairbanks, L. Labeyrie, D. Oppo, and N. Kallel, Deepwater source variations during the last climatic cycle and their impact on the global deepwater circulation, *Paleoceanography*, 3, 343-360, 1988.
- Einarsson, T., and K. J. Albertsson, The glacial history of Iceland during the past three million years, in *The Past Three Million Years: Evolution of Climatic Variability in the North Atlantic Region*, edited by N. J. Shackleton, R. G. West, and D. Q. Bowen, pp. 227-234, University Press, Cambridge, England, 1988.
- Epstein, S., R. Buchsbaum, H. A. Lowenstam, and H. C. Urey, Revised carbonate water isotopic temperature scale, *Geol. Soc. Am. Bull.*, 64, 1315-1326, 1953.
- Fairbanks, R. G., and R. K. Matthews, The marine oxygen isotope record in Pleistocene coral, Barbados, West Indies, *Quat. Res.*, 10, 841-844, 1978.
- Hodell, D. A., P. A. Mueller, J. A. McKenzie, and G. A. Mead, Strontium isotope stratigraphy and geochemistry of the late Neogene ocean (9 to 2 Ma), *Earth Planet. Sci. Lett.*, in press, 1989.
- Hulsemann, J., Notes: On the routine analysis of carbonate in unconsolidated sediments, *J. Sediment. Petrol.*, 36, 622-625, 1966.
- Imbrie, J., and J. Z. Imbrie, Modeling the climatic response to orbital variations, *Science*, 207, 943-952, 1980.
- Imbrie, J., J. D. Hays, D. G. Martinson, A. McIntyre, A. C. Mix, J. J. Morley, N. G. Pisias, W. L. Prell, and N. J. Shackleton, The orbital theory of Pleistocene climate: Support from a revised chronology of the marine  $\delta^{18}\text{O}$  record, in *Milankovitch and Climate*, Part 1, edited by A. Berger et al., pp. 269-305, D. Reidel, Hingham, Mass., 1984.
- Jansen, E., U. Bleil, R. Henrich, L. Kringstad, and B. Slettemark, Paleoenvironmental changes in the Norwegian Sea and the northeast Atlantic during the last 2.8 m.y.: Deep Sea Drilling Project/Ocean Drilling Program sites 610, 642, 643, and 644, *Paleoceanography*, 3, 563-581, 1988.
- Keigwin, L. D., Pliocene stable-isotope record of Deep Sea Drilling Project site 606: Sequential events of  $^{18}\text{O}$  enrichment beginning at 3.1 Ma, *Initial Rep. Deep Sea Drill. Proj.*, 96, 911-920, 1986.
- Kellogg, T. B., Paleoclimatology and paleoceanography of the Norwegian and Greenland seas: Glacial-interglacial contrasts, *Boreas*, 9, 115-137, 1980.
- Kennett, J. P., and S. Srinivasan, *Neogene Planktonic Foraminifera*, 265 pp., Hutchinson Ross, Stroudsburg, Pa., 1983.
- Klitgord, K. D., S. P. Huestis, J. D. Mudie, and R. L. Parker, An analysis of near-bottom magnetic anomalies: Sea-floor spreading and the magnetized layer, *Geophys. J. R. Astron. Soc.*, 43, 387-424, 1975.
- Kroopnick, P. M., The distribution of  $^{13}\text{C}$  of  $\Sigma\text{CO}_2$  in the world oceans, *Deep Sea Res.*, 32, 57-84, 1985.
- Krumsiek, K., and D. G. Roberts, Paleomagnetism of Tertiary sediments from the southwest Rockall Plateau, Deep Sea Drilling Project leg 81, *Initial Rep. Deep Sea Drill. Proj.*, 81, 837-853, 1984.
- Loubere, P., Gradual late Pliocene onset of glaciation: A deep-sea record from the northeast Atlantic, *Palaeogeogr., Palaeoclimatol., Palaeoecol.*, 63, 327-334, 1988.
- Mankinen, E. A., and G. B. Dalrymple, Revised geomagnetic polarity time scale for the interval 0-5 m.y. B.P., *J. Geophys. Res.*, 84, 615-625, 1979.
- Martinson, D. G., W. Menke, and P. Stoffa, An inverse approach to signal correlation, *J. Geophys. Res.*, 87, 4807-4818, 1982.
- Martinson, D. G., N. G. Pisias, J. D. Hays, J. Imbrie, T. C. Moore, and N. J. Shackleton, Age dating and the orbital theory of the ice ages: Development of a high-resolution 0 to 300,000-year chronostratigraphy, *Quat. Res.*, 27, 1-29, 1987.
- McDougall, I., and H. Wensink, Paleomagnetism and geochronology of the Pliocene-Pleistocene lavas in Iceland, *Earth Planet. Sci. Lett.*, 1, 232-236, 1966.
- Oerlemans, J., Model experiments on the 100,000-yr glacial cycle, *Nature*, 287, 430-432, 1980.
- Opdyke, N. D., and J. H. Foster, Paleomagnetism of cores from the North Pacific, *Mem. Geol. Soc. Am.*, 126, 83-119, 1970.
- Oppo, D. W. and R. G. Fairbanks, Variability in the deep and intermediate water circulation of the Atlantic Ocean: Northern hemisphere modulation of the southern ocean, *Earth Planet. Sci. Lett.*, 86, 1-15, 1987.
- Pisias, N. G., and T. C. Moore, The evolution of Pleistocene climate: A time series approach, *Earth Planet. Sci. Lett.*, 52, 450-458, 1981.
- Poore, R. Z., Temporal and spatial distribution of ice-rafterd mineral grains in Pliocene sediments of the North Atlantic: Implications for late Cenozoic climatic history, *Spec. Publ. Soc. Econ. Paleontol. and Mineral.*, 32, 505-515, 1981.
- Raymo, M. E., W. F. Ruddiman, and B. M. Clement, Pliocene-Pleistocene paleoceanography of the North Atlantic at Deep Sea Drilling Project site 609, *Initial Rep. Deep Sea Drill. Proj.*, 94, 895-901, 1986.
- Raymo, M. E., W. F. Ruddiman, and P. N. Froelich, Influence of late Cenozoic mountain building on ocean geochemical cycles, *Geology*, 16, 649-653, 1988.
- Ruddiman, W. F., and A. McIntyre, Ice-age thermal response and climatic role of the surface Atlantic Ocean,  $40^\circ\text{N}$  to  $63^\circ\text{N}$ , *Geol. Soc. Am. Bull.*, 95, 381-396, 1984.
- Ruddiman, W. F., and M. E. Raymo, Northern hemisphere climate regimes during the past 3 Ma: Possible tectonic connections, in *The Past Three Million Years: Evolution of Climatic Variability in the North Atlantic Region*, edited by N. J. Shackleton, R. G. West, and D. Q. Bowen, pp. 1-20, University Press, Cambridge, England, 1988.
- Ruddiman, W. F., M. Raymo, and A. McIntyre, Matuyama 41,000-year cycles: North Atlantic Ocean and northern hemisphere ice sheets, *Earth Planet. Sci. Lett.*, 80, 117-129, 1986a.
- Ruddiman, W. F., D. Cameron, and B. M. Clement, Sediment disturbance and correlation of offset holes drilled with the hydraulic piston corer: Leg 94, *Initial Rep. Deep Sea Drill. Proj.*, 94, 615-634, 1986b.
- Ruddiman, W. F., A. McIntyre, and M. Raymo, Paleoenvironmental results from North Atlantic sites 607 and 609, *Initial Rep. Deep Sea Drill. Proj.*, 94, 855-878, 1986c.
- Ruddiman, W. F., M. E. Raymo, D.G. Martinson, B. M. Clement, and J. Backman, Pleistocene evolution of northern hemisphere climate, *Paleoceanography*, this issue.
- Saltzman, B., Carbon dioxide and the  $\delta^{18}\text{O}$  record of late-Quaternary climatic change: A global model, *Clim. Dyn.*, 1, 77-85, 1987.
- Saltzman, B., and A. Sutera, A model of the internal feedback system involved in late Quaternary climatic variations, *J. Atmos. Sci.*, 41, 736-745, 1984.
- Saltzman, B., A. R. Hansen, and K. A. Maasch, The late Quaternary glaciations as the response of a three-component